COMPARISON OF THE MICROBIOLOGICAL INFLUENCE ON THE ELECTRO-CHEMICAL POTENTIAL OF STAINLESS STEEL BETWEEN MACRO AND MICRO AREAS OF SPECIMENS

O. Moos, P. Gümpel

HTWG, University of Applied Sciences Konstanz, Germany

Abstract

The micro-biologically caused ennoblement appears in natural waters on all stainless steels equally and has been described in numerous publications. In addition to an external polarization of such a system, temperature, oxygen and pH-levels, supply of nutrients and/or the supply of substances to restrain biological activity have a direct influence on the rate of the potential rise. The final value of the potential is substantially regulated by the biological system and is independent of the steel composition.

At the HTWG, University of Applied Sciences in Konstanz, Germany, the potential rise of stainless steels has been examined in experimental set-ups. Up to now, only effects on the open-circuit potential of specimens have been measured. In order to further understand the mechanisms behind the potential rise, these specimens have been divided into micro areas and *Microelectrodes* have been introduced to measure the electro-chemical potential of the micro areas. The experimental set-up not only allows for the mapping of the potential distribution over specimen surfaces, but further allows for learning more of the processes behind the rise of the electro-chemical potential.

Influences of availability of nutrients, biocides, oxygen and other factors on the free corrosion potential on the whole system as well as on the micro areas have been examined and compared. For example, use of biocides resulted in a rapid decrease of the free corrosion potential, however, only a very limited decrease of the potential within the micro areas could be measured. Experiments with an external polarization of the specimens resulted in similar curves with quantitatively different potential differences. This paper is to present the results of the conducted experiments and possible theories.

Introduction

In spite of the development of so called stainless steels, corrosion remains a huge problem up to this day. Several studies conducted in industrialized countries came to the conclusion that more than 4% of the gross domestic product (GDP) are lost due to corrosion, included the related cost for down time, every year. This means that the Federal Republic of Germany lost approx. 83 Mia. Euro due to corrosion in 2006. As it can be clearly recognized, the avoidance of corrosion and/or corrosion damages has a great economic value [1].

During the past 20 years, it has been described in numerous publications that micro-organisms can also indirectly attack metals and it is assumed that in up to 20% of all corrosion damages, micro organisms initiate or at least intensify the process [3-11]. This interaction between micro

organisms and corrosion is also sometimes described as MIC "Microbial Introduced Corrosion (MIC)", although this is not correct in the actual sense [3]. It is assumed that it is more a side effect caused by the presence of the micro organisms than the actual organisms themselves which lead to the actual corrosion. Therefore, MIC is also described as “Microbial Influenced Corrosion. One example is the fluctuation of the oxygen concentration in a bulk medium caused by the presence of aerobic organisms leading to corrosion [3].

The corrosion of metals is not a material property but the result of the interaction between the metal and the surrounding medium, and it must be regarded as a system property. Therefore, the condition of the metal surface has a substantial influence on the corrosion resistance. This means for the discussed stainless steels in water, highest resistance against corrosion attack is achieved with clean and blank metal surfaces [12-14]. Therefore, it is understandable that mirco-organisms attaching themselves on a metal surface and forming a biofilm have an effect on the system as a whole. The presence of the biofilm can act as a diffusion barrier, resulting in an accumulation of metabolic and corrosion products in the boundary layer biofilm/steel surface. The result is an influence on the well-known forms of corrosion and not in the appearance of new types of corrosion. One characteristic of microbial influenced corrosion is the promotion of pitting, shallow pit and crevice corrosion. It has been observed that a main characteristic for the occurrence of “Microbial Influenced Corrosion” on stainless steel in fresh water is the rise of the open-circuit potential (OCP). This effect is also called ennoblement.

Experimental Set-Up

A new experimental set-up has been developed, which allows for the reproducible examination of the potential raise of stainless steel caused by micro-organisms (Figure 1). It consists of several independent reactors with a volume of approx. 1.5 l each. A given quantity of an artificial salt solution can be pumped to the reactor continuously. This artificial salt solution is simulating the composition of the River Rhine and is used in order to exclude seasonal effects on the experimental set-up. The reactor is placed on an electro-magnetic stirrer allowing for the agitation of the content. All reactors are covered with an aluminium foil avoiding the influence of light on the experimental procedures. Connections installed in the covers of the reactors allow for the liquid exchange or aeration. Furthermore, small samples can be taken, reagents added and/or measurements performed (e.g. pH value and CO_2 content). The metal specimens are hung on wires, which are led through rubber plugs to keep the reactor gas-tight. The potential measurement takes place between the metal sample and an Ag/AgCl reference electrode, which is connected with the reactor by a salt bridge.

The potential raise is caused by inoculation of the experimental set-up with microbiological active sludge extracted from a cooling water system of a chemical company in Germany. The deliberate disturbance of the system by changing the availability of nutritions, changing the oxygen concentration in the salt solution, the addition of biocides and other substances, have showed that the system is reacting on a macroscopic scale.

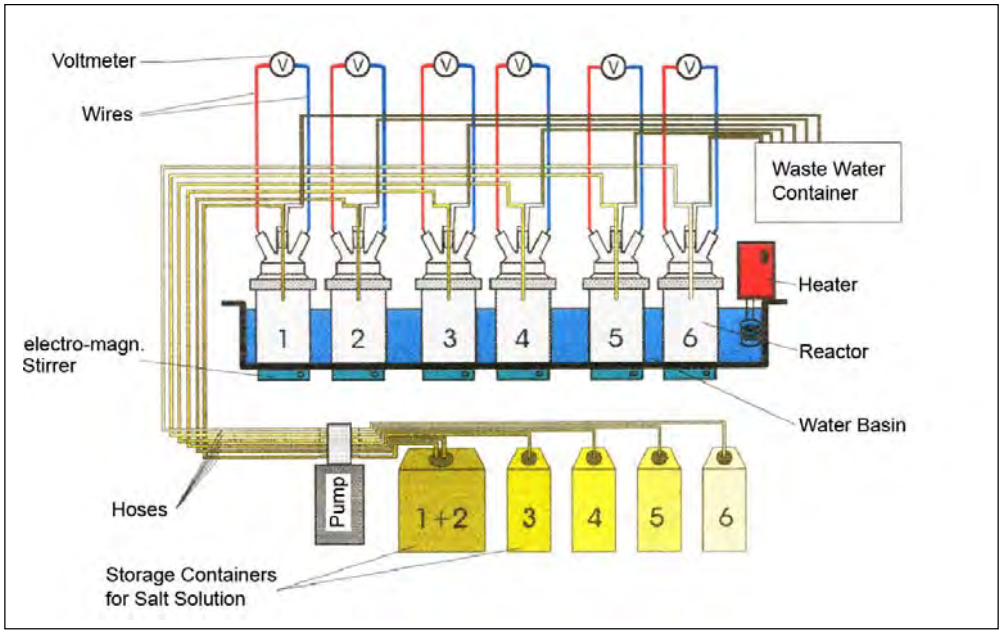

Figure 1. Schematicaly-out of the experimental set-up

The experiments performed proved that the final value of the potential is substantially regulated by the biological system and it is independent of the steel composition. Adding an optional source of nutrients (for example Ethanol) or strong biocides can suppress the potential raise and thereby avoid or reduce the risk of corrosion. However, the experimental set-up used up to this point of time, did not allow for obtaining information taht could explain the processes in the biofilm or at the boundry biofilm / specimen.

In order to further understand the mechanisms behind the potential rise, specimens have been divided into micro areas and microelectrodes have been introduced to measure the electro-chemical potential of these micro areas. The experimental set-up not only allows for the mapping of the potential distribution over a specimen surface, but further allows for learning more of the processes behind the rise of the electro-chemical potential.

Small deep-drawn stainless steel disks with a diameter of 25 mm and embedded microelectrodes made of stainless steel wire with a polyester coating were used as specimens (Figure 2). The arrangement was covered with a teflon disk to avoid direct contact of resin used for fixation and the salt solution.

Figure 2. Deep-drawn stainless steel disk with microelectrodes embedded in resin

Experimental Procedures

A few days after the inoculation of the reactor vessels and the development of a biofilm, the OCP reached values, which had been measured using the previous experimental procedures.

As only a limited time frame was available to conduct the experimental procedures, it was decided to stop the aeration with air and / or the flow of fresh salt solution to the reactor to intensify the environmental conditions during several experiments performed thereafter. Even though this was a deviation from the natural conditions, it still allowed for the quantitative interpretation of the results gained.

During the experimental procedures, the system was disturbed numerous times to evaluate the influence on the electro–chemical potential of both the macro and the micro areas. Instead of using air for the aeration, nitrogen was used to create anaerobic conditions, glucose, Potassium Cyanid and ethanol were added and, in one case, the whole experimental set-up was cathodically polarized.

It became quite obvious, that a change in the open–circuit potential did not automatically mean that the potentials of the micro areas revealed a concurrent and similar behaviour. In fact, in certain cases, the potential of the micro areas showed no effects whatsoever or a completely different behaviour. For instance, using nitrogen or ethanol resulted roughly in parallel curves for the OCP and the potential of microelectrodes.

The experiment with Potassium Cyanid was divided into two stages. In a first stage, 2 ml of 0.1 M KCN were added on a daily base (working days). The supply of fresh salt solution was stopped in order to intensify the conditions within the reactor. During this first stage, no reaction on any of the measured potentials could be attributed to the KCN. In fact, the OPC showed an increasing tendency, whereas the measured potentials of the microelectrodes indicated different tendencies from decreasing, being stagnant, ot to raising potentials (Figure 3).

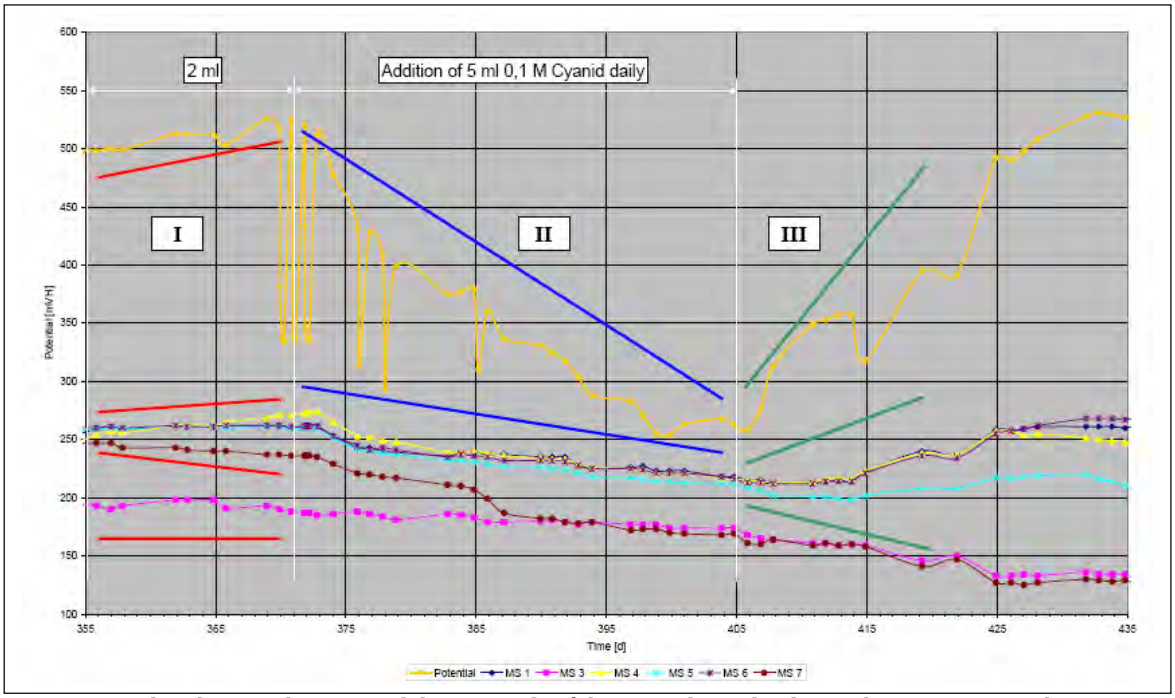

Figure 3. Graphic showing the OCP and the potentials of the microelectrodes during the experiment with Potassium Cyanid

Once the daily doses were increased to 5 ml of 0.1 M KCN, the OCP showed a decreasing tendency. This can be a result from the higher daily dose in addition to the fact that the accumulated amount of KCN in the reactor vessel reached a level, where it affected the microbiological system. However, whereas the OCP dropped by approx. 50% of its value, the potentials of the micro areas showed a decrease in the magnitude of approx. 20%.

The OPC recovered rather quickly after stopping the use of biocide and starting the exchange of the salt solution again. However, the potentials of the microelectrodes showed different tendencies. Some started to increase once again, while others showed a further decrease. This could be result from the dampening effect of the biofilm itself. It could also be caused by the placement of the microelectrodes on the specimen. Biofilms are not homogeneous, but include some channels as described by *Costerton* [16]. Depending on the distance between one of the channels and the microelectrode, reactions are noted earlier or later.

Besides the heterogeneous structure of the biofilm, different transport mechanisms within the biofilm could be an other explanation why the time for a response of the system was not always the same. Aeration with nitrogen or adding ethanol resulted in a change of all potential values measured within hours. On the other hand, it took several days in the case that glucose was added to see any reaction.

Furthermore, the arrangement of the experimental set-up might have an influence on the timing. For example, the total surface available to determine the OCP is in this case 184’000 times larger than the total surface of all microelectrodes combined.

Cathodic polarization of the experimental set-up resulted in the most dramatic and durable decrease of all measured potentials. The experimental set-up was cathodically polarized using a counter electrode. The potential of – 2.0 V was measured between the counter electrode and the reference electrode. The polarization took place over a period of 27 days. Whereas the OPC showed a drop of the polarization to a quasi-stable potential of approximately – 700 mV from the beginning, the potential measured within the micro areas showed a decreasing tendency.

These results have also been confirmed by recent findings published by Tanji *et al.* [17]. They state that the cathodic polarization causes “…an increased electrostatic repulsion between the steel surface and negatively charged bacteria”. An additional effect of a cathodic polarization is the increase in pH value.

After the cathodic polarization of the experimental set-up it was noticed that none of the potentials reached its values again as seen before.

Conclusions

A new experimental set-up has been developed, which allows for the reproducible examination of the potential raise of macro and micro areas of stainless steel caused by microorganisms. The goal of the research program described in this paper was to examine the effects of environmental changes in the system on the potential rise of specimens. Subsequently, Glucose, Potassium Cyanide and Ethanol were added to the reactors, aeration with Nitrogen and cathodic polarization of the experimental set-up were conducted.

With the selected research procedures new information on the mechanisms behind MIC could be obtained. As an example, the use of a biocide had a large influence on the potential of the large specimen, while practically no effect was shown up in the boundary layer biofilm/specimen.

Furthermore, it did not take long for the experimental set-up to recover. It could also be shown that anodic and cathodic areas are formed under the biofilm.

For future investigations, the experimental set-up can be modified to exclude the influence of the cylinder surface of the deep drawn disk. Likewise, the installation of a specimen with implemented microelectrodes into an industrial cooling water system would allow for the collection of data under “real life” conditions.

References

[1] Internet: RWTH Aachen. Institut für Eisenhüttenkunde. Korrosion und Oberflächen, in: http://wh2.iehk.rwth-aachen.de/lehre/werkstofftechnik/oberflaechen_korrosion/. (10.04.2004).

[2] W. Dietzel: “Korrosion metallischer Werkstoffe“, Spektrum der Wissenschaft. July 1998, pp. 96-100.

[3] E. Heitz, H.-C. Flemming, W. Sand: “Microbially Influenced Corrosion of Materials”, Springer Verlag, Berlin, 1996.

[4] P. Gümpel, M. Kässer, R. Kreikenbohm: “Korrosion durch Mikroorganismen“ Spektrum der Wissenschaft, July 1998, pp. 108.

[5] S. Watkins Borenstein: “Microbiologically influenced corrosion handbook”, Industrial Press, Inc. 1994 .

[6] Guidelines for the Selection of Stainless Steels for Marine Environments, Natural Waters and Brines. A Nickel Development Institute Reference Book Series N° 11 003. 1987.

[7] U. Eul: “Entwicklung und Einsatz einer Simulationsapparatur zum Nachweis und zur Verhinderung von mikrobiologisch beeinflusster Korrosion (MIC)“, Dissertation, Johann Wolfgang Goethe–Universität in Frankfurt am Main. 1997. pp. 1 – 2.

[8] U. Heubner: “Mikrobiologisch beeinflusste Korrosion nichtrostender Stähle und ihre Vermeidung“. Chemieingenieurtechnik, Vol. 72, 2000, pp. 1439-1444.

[9] D. Thierry: “Aspects of microbially induced corrosion”, EFC by the Institute of Materials 1997.

[10] J. Korkhaus, J.T. Titz, G.H. Wagner: “Lochfraß an Flusswasser- Rohrleitungen aus hochlegierten austenitischen nichtrostenden Stählen“, Werkstoffe und Korrosion 45, 1994, pp. 87 – 95.

[11] M.H.W. Renner, G.H. Wagner: “Microbiologically Induced Corrosion (MIC) of Stainless Steels”, Proc. Int. Conf. Stainless Steels'96, 2nd European Congress. Düsseldorf/ Neuss. June 03 – 05. 1996. Verlag Stahleisen GmbH. Düsseldorf. 1996. pp. 411-417.

[12] P. Gümpel: “Rostfreie Stähle“, Expert Verlag. Renningen. 1996.

[13] H. Kaesche: “Die Korrosion der Metalle“, Springer-Verlag Berlin, Heidelberg, New York, London, Paris, Tokyo, Hong Kong, Barcelona. 1990.

[14] A.S.M. Diab, W. Schwenk: „Beeinträchtigung der Lochkorrosionsbeständigkeit von CrNi-Stählen durch dünne Oxidschichten“, Werkstoffe und Korrosion, 44, 1993, pp. 367-372.

[15] J.W. Costerton et al.: “Biofilms, the Customized Microniche”, Journal of Bacteriology, 1994, pp. 2137-2142.

[16] Y. Tanji et al.: “Effect on cathodic protection on biofilm formation and maturation” NACE International, Corrosion 2007. Paper 07513. 2007. pp. 1-8.

CORROSION DAMAGE OF COMPRESSOR BLADES FROM GRADE 14Cr17Ni2 STAINLESS STEEL

V. Číhal[1], E. Kalabisová[2], R. Štefec[3], L. Turek[2]

[1]VSB - Technical University Ostrava, Czech Republic, [2]SVUOM Ltd., Czech Republic, [3]Czech Technical University, Czech Republic

Abstract

A special electrochemical corrosion test, EPR – potential polarization reactivation confirmed the link between damage to compressor blades by fracture mechanics and their corrosion damage. Due to an excessively vigorous grinding and polishing the blades suffered a thermal exposure in areas near the blade base where the steel 14Cr17Ni2 became locally overheated to a temperature of ca. 550°C, causing a significant sensitization to corrosion attack at grain boundaries, whereupon the blades failed by a fracture mechanism.

KEYWORDS: EPR test, martensitic steel, intergranular corrosion, turbine blade, failure

Introduction

In special cases, the behavior of material in terms of fracture mechanics may be closely related to a damage suffered by the material due to corrosion. The closeness of this link can be documented by a case which occurred in practice: compressor blade made of grade 14Cr17Ni2 steel suffered localized corrosion attack near the blade foot in areas previously ground and polished.

The electrochemical potentiodynamic reactivation method – EPR test – came as a response to a situation in corrosion testing which was primarily characterized by the need for a better, quantitative method of measuring the degree of sensitization in welded components and the need for a rapid, non-destructive field test.

The EPR test is a direct method of potentiodynamic measurement where the measured response is an integral curve in the sense that the current density coordinate of the polarization plot corresponds to the algebraic sum of all oxidative and reductive processes taking place on the surface of the working electrode under study [1]. Double-loop EPR, applied in the present case study, is a bidirectional, 'cyclic' sweep consisting of a forward scan followed by a reverse scan, possibly with a delay at vertex which generally is located within the passive range. Various quantities (mainly, characteristic potentials, currents and coulombic charges) are recorded and interpreted as relating to the different corrosion types studied, but they all derive from the shape of the EPR curves measured.

Basically, EPR consists in evaluating a potentiodynamic scan of the material being tested, the scan(s) being conducted so as to satisfy certain conditions linked to the surface properties of the material (Figure 1). In fact, two variants have become common, *viz*., the single loop scan and the double loop scan, of which the latter appears to offer a higher corrosion resolution potential.

Prominent applications of the EPR technique include a variety of alloys and their phases in various corrosion environments.

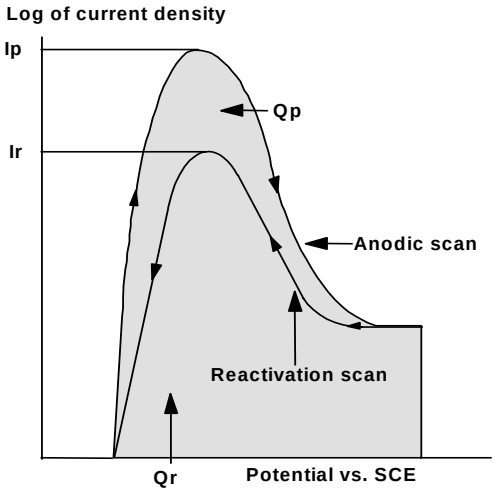

Figure 1. Schematic polarization curves for the double loop EPR test

The gist of the problem

The corrosion failure case described below concerns the blades of a high-power air compressor. It was suspected from the outset that the corrosion damage observed had not been produced while the compressor was running but, to the contrary, during a period of compressor shutdown. The corrosion medium responsible was the condensate – produced by condensation from humid air. Certain areas of the blades, dismantled from the compressor after a period of operation, were found to have suffered corrosion damage of intergranular character. Also, fatigue tests performed on the blades indicated inadmissible, too low values of the fatigue limit in some cases. The fatigue fracture surface showed certain amounts of intergranular facettes. It had been presumed initially that the low fatigue limit might be related to some early-stage manufacturing operations where in certain cases, extensive cracks of markedly intergranular character were found, the material also exhibiting catastrophic local reductions of notch toughness. It was initially believed that the damage suffered at the points of transition between the blade proper and its base was due to a fatigue mechanism or that possibly, so-called corrosion fatigue was involved. Eventually however, the examination of the affected areas – also relying on previous experience from research of austeno-martensitic steels [2,3] – led us to suspect a different mechanism, *viz.*, that at the transition between the blade root and the blade the pressures applied during the grinding and polishing operations were excessive, provoking a primary sensitization to corrosion in the material where the temperatures reached the danger zone of 400-600°C, *i.e.*, that the material became corrosion-sensitive due to local overheating.

The compressor suffered damage both on the rotor blades and on the stator blades (Figures 2 and 3). The fact that stator blades were also attacked (Figure 3) made it clear that fatigue could not have been the decisive factor contributing to corrosion.

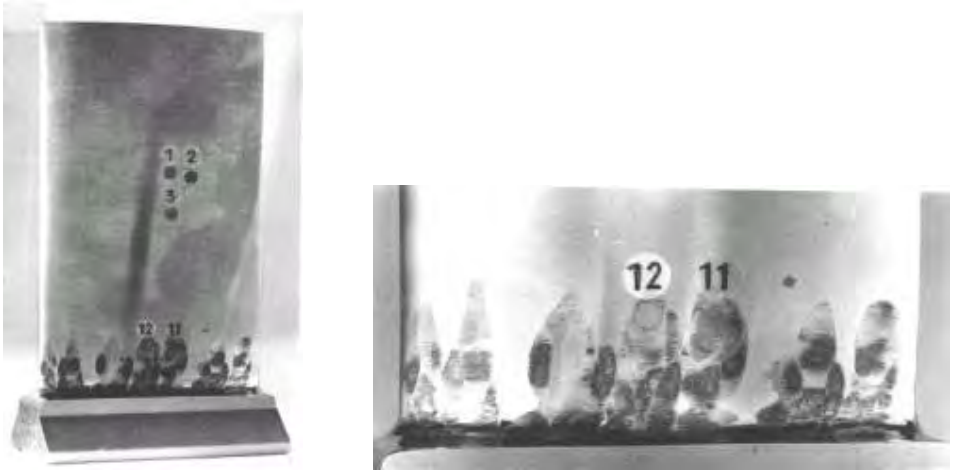

Figure 2. Corrosion damage on rotor blade indicating EPR test locations view of entire blade (left) and detailed view of blade base (right)

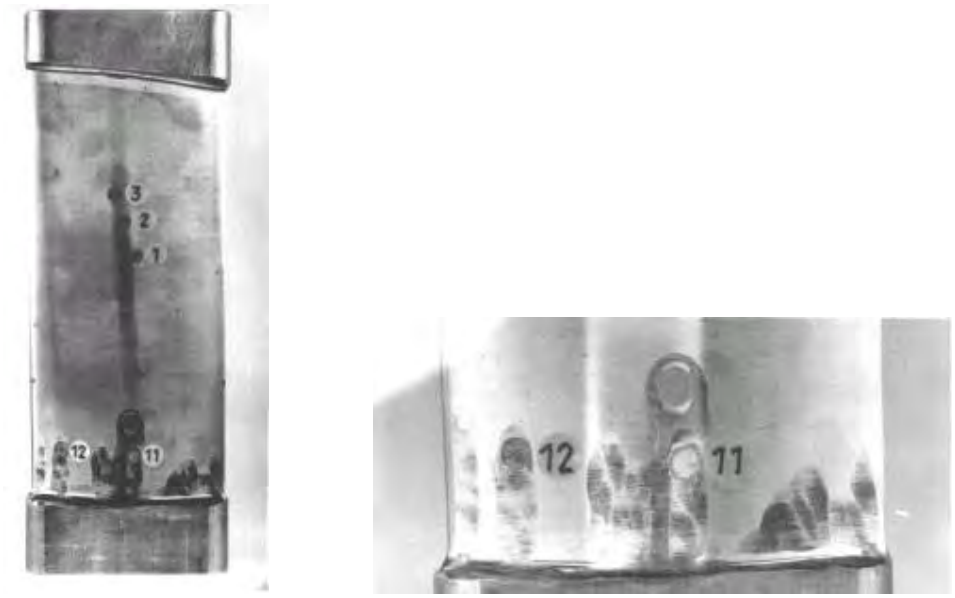

Figure 3. Corrosion damage on stator blade indicating EPR test locations view of entire blade (left) and detailed view of blade base (right)

Experimental

The method chosen to examine the cause underlying this damage was EPR – electrochemical potential reactivation [4]. The EPR technique was applied *in situ* to the locations identified in the Figures 2a, 2b.

The temperatures of 500 - 550°C are critical inducing a sensibilisation in these martensitic steels. Therefore, two kinds of specimens were tested: the blade material in the "singed" areas and, additionally, special specimens previously heat-sensitized by exposure to the above critical range of temperatures, which were also subjected to the electrochemical corrosion tests. Three series of these comparative specimens were fabricated: one series was tempered at the temperature of 380°C, the second one at 550°C and the third one at 680°C, always for a period of 4 hours. All these specimens were 23 by 10 by 133 mm in size, with as-ground surface. The results of this tests are given in Table 2.

The medium used for the potentiodynamic measurements was 0.5M H_2SO_4 + 0.01% KSCN, and the measurements were carried out on both the blade samples and the comparative specimens, at a potential scan rate of 250 mV/min. and a temperature of 25°C. The quantities recorded were the critical passivation current density J_p, the reactivation current density J_a, the coulombic charge passed during activation and passivation C_p, and the coulombic charge passed during reactivation C_a.

Additionally, the comparative specimens were also subjected to immersion tests by exposure to 20% acetic acid, to 5% nitric acid, and to so-called standard (Strauss) solution for testing the susceptibility to intergranular corrosion, *i.e.*, $H_2SO_4 + CuSO_4 + Cu$. The values of corrosion due weight loss were recorded and subsequently expressed as corrosion rates in g/m^2h and to mm/year.

Results

The results of the potentiodynamic tests run on the heat-affected surfaces of the blades are given in Table 1. The measurements from the test locations 11 and 12 are from the hard grining zones before polishing blades. The measurements from the locations 1, 2 and 3 are from the fine grinded and polished center of the blades. On the rotor blade in the case of points 12 and 3 and on the stator blade in the case of all points the consecutive runs are taken during the measurements.

The tests results obtained from the "singed" areas are summarized in Table 1.

Table 1. Potentiodynamic measurements on heat-affected surfaces of the blades

component	test location		J_p mA cm^{-2}	J_a mA cm^{-2}	C_p C cm^{-2}	C_a C cm^{-2}	C_a/C_p
rotor	base	11	22.0	7.9	0.972	0.280	28.8
		12	180.0 19.6	7.4 6.4	0.674 0.700	0.204 0.170	30.2 24.3
	blade	1	14.0	0.30	0.328	0.0	0.0
		2	13.0	0.16	0.304	0.0	0.0
		3	190.0 19.3	0.60 0.62	0.616 0.636	0.006 0.006	0.97 0.94
stator	base	11	32.0 34.0	11.4 8.0	1.502 1.478	0.360 0.248	24.0 16.8
		12	35.5 36.0	10.2 7.0	1.570 1/530	0.314 0.200	20.0 13.0
	blade	1	29.0 33.0 34.0	6.2 5.2 5.4	1.090 1.222 1.226	0.152 0.120 0.124	13.9 9.8 9.6
		2	30.0 25.5	5.6 6.0	1.172 1.316	0.142 0.172	12.1 13.1
		3	36.0 34.0	5.0 4.7	1.338 1.308	0.118 0.110	8.8 8.4

Generally, the "singed" areas exhibit high values of the coulombic reactivation ratios C_a/C_p, which are a warning flag attesting to the presence of an increased corrosion sensitiveness due to the precipitation of chromium carbides and sensibilisation;

These measurements make it clear that the primary cause of the corrosion due to the damage of the blades was overheating during grinding in some regions. This is confirmed by the fact that the intensity of attack fades off with increasing depth under the surface. Grinding produced high

temperatures mainly at the blade surfaces, whereas at greater depths the temperatures reached must have been lower.

The results given in Table 1 on heat treated (sensitized) specimens indicate that replicated potentiodynamic measurements run at the same point of the heat-affected surface always give lower reactivation ration values, indicating that the "signed" surface has been removed, causing the effect of overheating to fade away as the subcutaneous layers of the steel are exposed. In repeated potentiodynamic measurements conducted on the same surfaces after prudent grinding and polishing this negative effect *i.e*, sensitization due to overheating, falls off gradually, due to the removal of the original (most affected) surface layer.

The measurements on the heat treated specimens (Table 2) acknowledge the sensitization influenced by critical temperature 550°C of this 14Cr17Ni2 stainless steel.

Table 2. Potentiodynamic measurements of heat treated (sensitised) specimens

heat treatment	**run no.**	**J_p** mA cm^{-2}	**J_a** mA cm^{-2}	**C_p** C cm^{-2}	**C_a,** C cm^{-2}	**C_a/C_p**
380°C/4hrs	3a	29.0	7.4	0.950	0.150	18.1
	3b	34.0	12.4	0.996	0.258	25.9
	3c	32.4	12.4	1.120	0.270	24.1
550°C/4hrs	4a	51.0	42.0	2.000	1.100	**55.0**
	4b	53.0	42.0	2.110	1.132	**53.5**
	4c	50.0	41.0	2.022	1.176	**57.4**
680°C/4hrs	5a	56.0	11.7	2.486	0.280	11.2
	5b	62.0	21.0	2.764	0.528	19.1
	5c	59.5	23.5	2.706	0.636	23.5

The measurements denoted as a, b, and c are always three consecutive runs performed at the same point of the surface of a specimen heated at a given temperature. The values of the reactivation ratios C_a/C_p obtained clearly indicate that the temperature of 550°C is critical with this material, yielding the highest C_a/C_p values (shown in bold font). Even the temperature of 380°C provokes grain boundary sensitization, where preferential attack may occur. On heating at the highest temperature tested, 680°C, the level of sensitization at grain boundaries is lowest.

The results of the immersion tests of corrosion are given in Table 3.

The trend is the same again – the negative effect of thermal exposure to 550°C is clearly discernible. This applies to exposure in all the three test solutions. The pertinent (highest) corrosion rate is shown in bold in the Table 3.

Table 3. Results of immersion tests of heat treated (sensitized) specimens

test environment	heat treatment	g m^{-2} h^{-1}	mm/year
standard solution, boiling, 24 hrs	380°C/4h	0.127	0.142
	550°C/4h	62.299	**69.966**
	680°C/4h	0.212	0.238
CH_3COOH 20%, boiling, 24 hours	380°C/4h	0.028	0.032
	550°C/4h	8.404	**9.439**
	680°C/4h	0.642	0.721
HNO_3 5% 24 hrs, 20°C	380°C/4h	0.011	0.012
	550°C/4h	0.319	**0.358**
	680°C/4h	0.051	0.057

Discussion

Penetration of intergranular attack along the original austenite grains produced by tempering may be observed in other martensitic steels such as Cr17Ni2, as is also demonstrated by EPR measurements (Figure 4).

To obtain yet another proof of the existence of this corrosion effect, and also to check on whether it is indeed true that this steel will not withstand an exposure to the temperatures of 500-600°C, the potentiodynamic measurements were also performed on the heat treated (sensitized) specimens of the comparative series (Figure 4, Table 2).

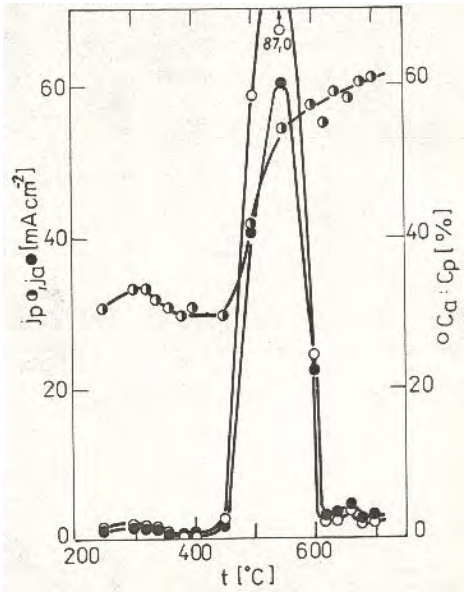

Figure 4. Critical passivation current density j_p, reactivation current density j_a, and the ratio of reactivation charge to passivation charge (C_a/C_p) as function of annealing temperature (4 hrs) for 14Cr17Ni2 steel

Grade 14Cr17Ni2 steel generally has a tendency to become sensitized to intergranular attack by a number of factors – the corrosion environment, applied mechanical loads, internal stress, etc. The same effect of the tempering temperature on the critical passivation current density J_p and the Q_a / Q_p ratio was observed [2] on quenched-and-tempered martensitic 14Cr17Ni2 stainless steel (quenched at 1040°C/3min./oil and tempered for 4 h) as revealed by earlier EPR measurements conducted in 0.5M H_2SO_4 + 0.01 % KSCN at ambient temperature, at a scan rate of 15 V . h^{-1}.

This tendency to sensitization is directly linked to the character of structure at the boundaries where ferrite δ interfaces with martensite, and the primary grain boundaries are influenced mainly by the redistribution processes involving the carbidic phase during the processing cycles which produce thermo-mechanical exposure. The resultant phenomena exhibit the character of temper brittleness. Susceptibility to intergranular damage is inherent in the very metallurgical design of this steel grade, and can become strengthened by certain fluctuations of the steelmaking and fabrication processes applied – also including the rather inconspicuous but despite of this, too vigorous grinding and polishing.

Conclusions

The study of grade 14Cr17Ni2 steel destined for compressor blades has resulted in the following conclusions:

- The corrosion resistance of the steel is greatly reduced by thermal exposure to temperatures within the range of 500-600°C, causing considerable reactivation due to grain boundary sensitization to preferential attack.
- The results obtained on heat treated specimens by the potential polarization method are well-compatible with the behavior o the heat-affected blades.
- Susceptibility to preferential intergranular attack after exposure to temperatures around 550°C was confirmed by immersion tests of corrosion.
- The potential polarization reactivation method has proven to be a tool well-suited to ascertaining the optimum conditions of treatment for martensitic stainless steels and can also serve as a nondestructive measuring technique.

These results highlight the fact that in fracture mechanics studies, it occasionally pays off also to concentrate upon the corrosion effects to which the material under study is being subjected, in as much as both these mechanisms – fracture mechanics as well as corrosion attack – may act in a concerted manner and may even strengthen each other when acting on the material. Thus, for the sake of a satisfactory, rational explanation of these phenomena, it may be expedient to combine the interpretative capabilities of fracture mechanics and corrosion engineering.

Acknowledgment

The work was undertaken within the context of CR Grant agency project GACR #106/08/1789 and Ministry of Education project MSM #2579478701.

References

[1] R. ŠTEFEC, “Corrosion data from polarization measurements”. Ellis Horwood, London, ISBN 0-13-173725-2, 386 pp. (1990)
[2] V. ČÍHAL, J. JEŽEK, “Kovové materiály VI” (1968) pp. 441-51; Jernkontorets Annaler 153 (1969) 153-157
[3] V. ČÍHAL, J. HUBÁČKOVÁ, J. KUBELKA, K. MAZANEC, “Materials Chemistry & Physics 11” (1984) 279-93.
[4] V. ČÍHAL, T. SHOJI, V. KAIN, Y. WATANABE, R. ŠTEFEC: “EPR — a comprehensive review”. Tohoku Univ., Sendai, Japan (2002) 142 s.

CHANGES OF SURFACE MORPHOLOGY OF FERRITIC STAINLESS STEELS AT HIGH-TEMPERATURE OXIDATION

M. Malinina, M. Gasik

Helsinki University of Technology, Finland

Introduction

Stainless steels are being widely used as structural materials for interconnects in solid oxide fuel cells (SOFC) and similar applications with aggressive environments operating at high temperatures. Oxidation, hot corrosion and erosion affect the performance and lifetime of SOFC interconnects. Formation of an oxide layer on the steel surface can protect it from failure atmosphere. The protective oxides may have low conductivity, and the growth of these oxides is limited because these oxides act as a diffusion barrier between the material and the atmosphere. The effect of various environments on the oxidation behaviour of stainless steels has been investigated for traditional applications [1-5] and formation of spinel was considered as a good compromise between oxidation protection and electrical resistance requirements.

The study of the ferritic alloy Crofer 22APU indicated the formation of a layered oxide comprised of a chromia-rich sublayer and $(Mn,Cr)_3O_4$ spinel-rich top layer at its oxidation at 800°C in air at different times [2]. During the early stages of oxidation, both chromia and spinel phases nucleated on the alloy surface and grew with preferred crystallographic orientations. With time, the separate spinel crystallites began to coalesce, and the scale microstructure became homogenized. Continued oxidation led to the growth of a chromia-rich scale beneath the spinel rich layer, resulting in two compositionally distinct oxide layers.

The oxide scales formed on all studied commercial ferritic steels oxidized at 800°C in air for 100-1000 h consists of external $MnCr_2O_4$ spinel layer and a "sub-scale" of Cr_2O_3 oxide [3]. The oxide surface morphology for the alloys containing titanium and lanthanum is very similar, with the presence of decoration at the alloy grain boundaries due to the formation of titanium internal oxides. When these alloys are oxidized in air, a slightly increase in the oxidation rate was observed for those alloys with Ti and La additions, due mainly to the formation of pronounced titanium internal oxides at the alloy grain boundaries, forming a buckled oxide scales, but no detachment from the alloy surface was observed. The alloys without those additions form a relative smooth oxide scale without internal oxide formation, showing a better oxidation resistance [3].

Ferritic stainless steel AISI 430 was investigated after heating at 800°C for 300 h in air and in dual atmosphere [4]. Microstructural and EDX analyses indicated that the scale grown during heating was comprised of manganese $(Mn,Cr,Fe)_3O_4$ rich top layer and Cr_2O_3 rich sublayer. Occasionally, a thin silica film was observed between the chromium and manganese-rich scale and the alloy substrate. The oxidation behaviour (scale growth and composition) on the air/fuel-side was found to be different from the behaviour observed when the steels are exposed to air only. SEM observation of scale surfaces confirmed that both scales had similar composition and microstructure, with MnO crystals on a spinel-rich substrate, and a silica layer lying beneath the spinel-rich layer. From the point of view of contact resistance, formation of SiO_2 or Cr_2O_3 layers may be considered as a disadvantage.

Ferritic stainless steels like ITM 14, ZMG232, 446 and Crofer 22APU were studied after oxidation tests at 800°C in air for 5000 h [5]. Mass gain vs. time derived from oxidation showed compatible behaviour where mass changes were <2.25 mg/cm^2. ZMG232 was more subjected to oxidizing process and as consequence to change. For comparison, change of weight of others steels was within the limits of 0.5-1.5 mg/cm^2 [5].

Experimental

Several ferritic stainless steels (types 430, ITM14 (Plansee), ZMG232 (Hitachi), Crofer 22APU (Thyssen Krupp)) were studied in this work. Steel plates were cut in cubes ~15 x 15 x 2-3 mm and polished with SiC paper 800 grit. The chemical composition of alloys is shown in Table 1. Chromium equivalent (ECr) was calculated using conventional rules for stainless steels.

Table 1. Alloys chemical composition, % wt.

	Cr	Ti	Zr	La	Mn	Mo	Si	Y	ECr
430	16.5				1.0		1.0		*18.0*
ITM14	26.85	0.3			0.4	2.3	0.03	0.2	*29.2*
ZMG232	22.1		0.22	0.044	0.5		0.4		*22.7*
Crofer 22APU	22	0.08		0.08	0.4		0.11		*22.2*

The first experiments for high-temperature oxidation were carried out at 800°C during 168-170 h (1 week) in static air. The next series were done at 900°C and 1000°C for 24 h in static air. All specimens were weighed before and after furnace tests and their weight change was analysed. After measurements, sample surfaces were studied by SEM.

Results

Growth of oxide layer (at high-temperature oxidation) was visually observed in all specimens. The thickness and structure of this layer depend on the steel composition and temperature. A significant difference in oxidation resistance over 800°C between studied steels has been observed (Figure 1).

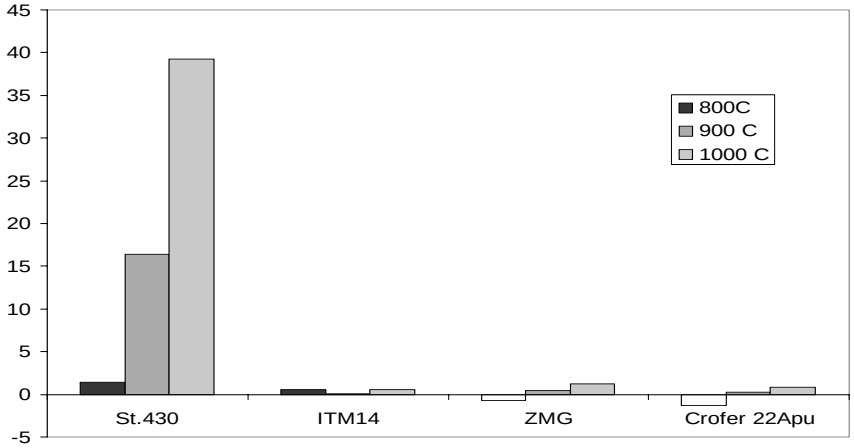

Figure 1. Weight changes after high-temperature oxidation in air (168 h at 800°C, others 24 h)

In air ferritic stainless steels show compatible behaviour except for mass changes, which were in the +40 mg/cm^2 limits for steel 430 and ±1.5 mg/cm^2 for others. These data are in agreement with literature data where available. Negative mass changes are normally associated with

chromia and $CrO(OH)_2$ evaporation, but this does not immediately correlate with chromium content neither with ECr value (Table 1).
Surface morphology of steel 430 (800°C, 170 h) shows a uniform layer of octahedral crystals with hexagonal wafers ("chips") in some places; they are nearly perpendicular to the surface and are concentrated in relatively narrow areas (Figure 2a). According to SEM microanalysis, the hexagonal wafers are nearly pure Cr_2O_3, the octahedral crystals are mainly spinels based on $(Mn,Cr)(Cr,Mn)_2O_4$. The uniform layer of such octahedral crystals is also typical for ITM14, ZMG232 and Crofer 22APU steels (Figure 2b).

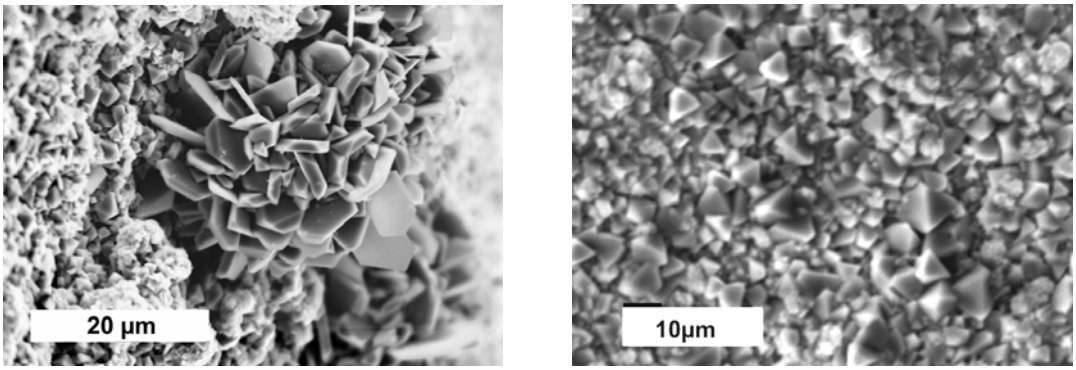

(a) (b)

Figure 2. Surface morphology of steel 430 (a) and ZMG232 (b) after oxidation in air (800°C, 170 h).

Observation of steels surface compositions at higher temperatures shows significant differences between them. At higher temperatures the scale surface became more homogeneous and spinel phase disappears at 430 and ITM14 specimens (Figure 3). For 430 steel at 900°C a specific surface profile with oxide "pinches" growing in different directions can be seen but at 1000°C surface became smoother. The microanalysis of samples confirms oxides as Fe_3O_4 and Me_2O_3 but no spinel was found here.

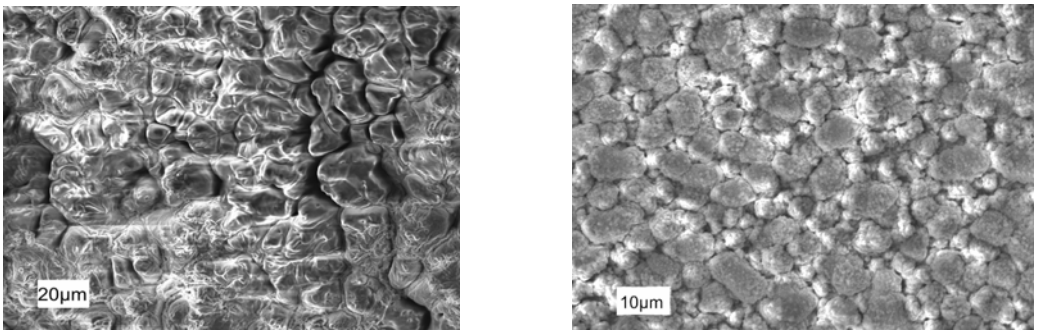

(a) (b)

Figure 3. Surface morphology of steel 430 (a) and ITM14 at 1000°C after 24h exposure.

Crofer 22APU and ZMG232 steels show other tendency. There are spinel phases at all temperatures studied (800, 900, 1000°C). At increased temperatures significant growth of octahedral crystals was found (Figure 4). SEM examination of the surface indicated octahedral crystals as spinels based on $MnCr_2O_4$ and the large octahedral crystals could be mixed oxide $(Cr,Mn)_2O_3$.These spinels and mixed oxides have distinctly different Cr/Mn ratios vs. temperature and original steel compositions ($(Cr,Mn)_2O_3$ had very little manganese, so it was not considered for further analysis). In order to find this correlation, spinel compositions of these oxide layers of the steels were located onto the Mn_2O_3 - Cr_2O_3 phase diagram [10].

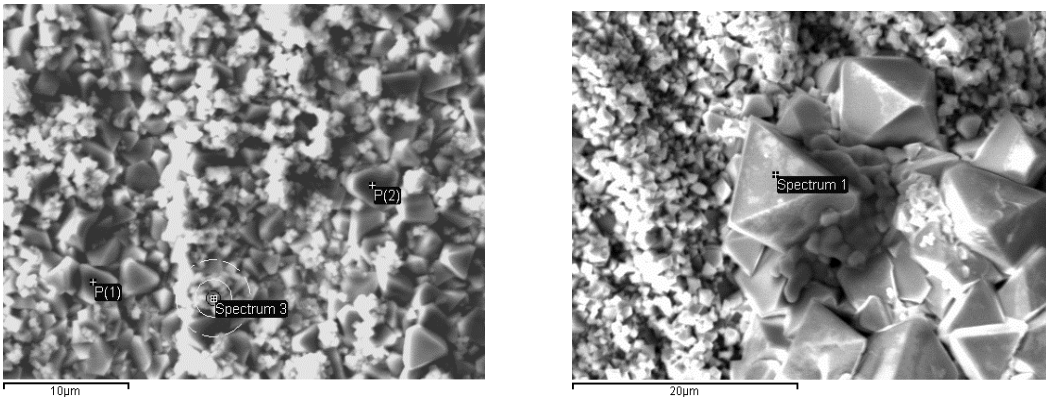

(a) (b)

Figure 4. SEM examination of the steel surface ZMG232 at 900°C, 24h (a) and Crofer 22APU at 1000°C, 24h (b).

All these steels have spinel formation at 800°C with composition varied by increasing Mn fraction in order Crofer > ZMG > ITM > 430. Steels 430 and ITM14 ceased to form distinct spinels at 900-1000°C, whereas Crofer has the most steady spinel composition (Cr/Mn = 1…1.5). ZMG232 produces nearly stoichiometric spinels at 900°C (Cr/Mn ~2) but more close to hausmanite at 1000°C (Figure 5). It is not clear, whether this is caused by a higher Mn content in ZMG vs. other equivalent steels or by impact of minor alloying elements (even higher Mn content in 430 does not count due low chromium content in this steel). Except for small titanium contents, no active elements (La, Zr, Y) were found in oxides or in spinels during EDX analysis of surface scale at all sites.

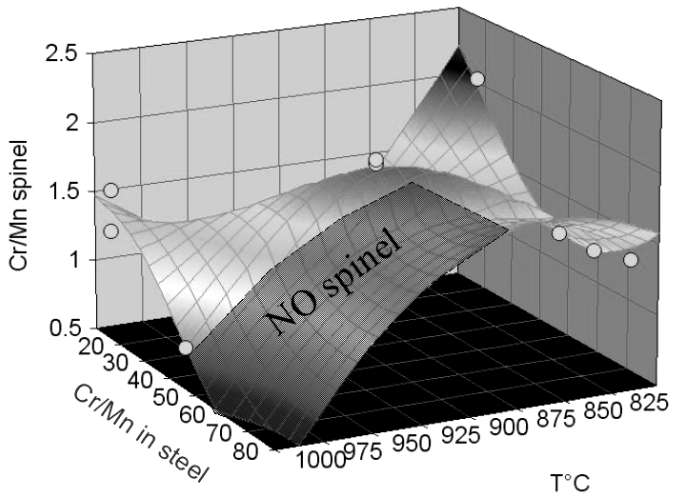

Figure 5. Molar ratio Cr/Mn in spinels [10] vs. oxidation temperature and initial Cr/Mn ratio in steels.

During oxidation a depletion of the scale forming elements, mainly Cr, leads to a change in the composition of the surface scale and consequently also to a change in the oxide growth rate. Lower initial concentration of chromium in the alloy (< 20%) leads to a slight increase of the oxidation rate. Not only depletion of chromium, but also manganese is responsible for this oxidation behaviour. Manganese is known to play an important role in the oxidation mechanism of the ferritic steels and, due to its low concentration, it will exhibit completely different depletion kinetics as chromium [11].

Although Cr/Mn ratio in spinels does not explicitly correlate with oxidation temperature neither equivalent chromium content, it seems that “good” spinel formers for initial stages of oxidation are ferritic steels with ECr ~21…24, low titanium and increased manganese.

Conclusions

The oxidation behaviour of ferritic stainless steels have been studied in the temperature range 800-1000°C in static air for 24-168 hours. A significant difference in oxidation of these steels has been observed. Mass changes were in the +40mg/cm^2 limits (steel 430) and ±1.5 mg/cm^2 for all others.

Surface observation of the air oxidized specimens by SEM show the differences in oxide layer formation. Chromia- and spinel-rich layers (as well as single crystallites) were observed for all steels at 800°C. At higher temperatures (900 and 1000°C) the growth of spinel with different composition was found for ZMG232 and Croffer22APU only. Alloys 430 and ITM14 showed at these temperatures only oxides like Me_2O_3. The effect of active element additions (La, Zr, Y) was not directly observed in this study neither they were found in oxides or in spinels. "Good" spinel formers for initial stages of oxidation are ferritic steels with ECr ~21…24, low titanium and increased manganese, whereas processing for thermally grown spinel is likely better to carry out at elevated temperatures (over 900°C) but with shorter times.

Acknowledgments

Financial support of this research by the Outokumpu Foundation is gratefully acknowledged.

References

[1] M. Schutze, Ed. John Wiley & Sons Ltd., Baffins Lane, Chichester, England (1997).

[2] Z. Yang, J.S. Hardy, M.S. Walker, G. Xia, S.P. Simner and J.W. Stevenson, "Structure and conductivity of thermally grown scales on ferritic Fe-Cr-Mn steel for SOFC interconnect applications", J. Electrochem. Soc., 151, (11), A1835-A1831, (2004).

[3] F.J.P. Abellan, W.J. Quadakkers, "Development of ferritic steels for application as interconnect materials for intermediate temperature solid oxide fuel cells (SOFCs)", Forschungszentrum Julich, (2005), 206 p.

[4] Z. Yang, M.S. Walker, P. Singh and J.W.Stevenson, "Anomalous corrosion behavior of stainless steels under SOFC interconnect exposure conditions", Electrochemical and Solid-State Letters, 6 (10), B35-B37, (2003).

[5] A. Venskutonis, W. Glatz and G. Kunschert, "P/M Processing of ODS Cr- and FeCr-based alloys for solid oxide fuel cell applications", Proc. 16th Plansee Seminar Vol. 1, (2005), 534-544.

[6] P. Kofstad, "High-temperature corrosion", Elsevier, Amsterdam (1988).

[7] Z. Yang, K.S. Weil, D.M. Paxton and J.W. Stevenson, "Selection and evaluation of heat-resistant alloys for SOFC interconnect applications", J. Electrochem. Soc., 150, (9), A1188-A1201, (2003).

[8] T. Brylewski, M. Nanko, T. Maruyama, K. Przybylski, "Application of Fe-16Cr ferritic alloy to interconnector for a solid oxide fuel cell", Sol. St. Ionic, 143, (2001), 131-150.

[9] K. Huang, P.Y. Hou, J.B. Goodenough, "Caracterization of iron-based alloy interconnects for reduced temperature solid oxide fuel cells", Sol. St. Ionic, 129, (2000), 237-250.

[10] Yu.V. Golikov, S.Ya. Tubin, D.V. Bamburov, V.F. Balakirev, "The system MnO-Cr_2O_3-Mn_2O_3", Mater. Sci. Monogr., 38A (High Tech. Ceram., Pt. A) 237-246 (1987).

[11] P. Huczkowski, N. Christiansen, V. Shemet, J. Piron-Abellan, L. Singheiser, W.J. Quadakkers, "Oxidation limited life times of chromia forming ferritic steels", Mater. and Corrosion, 55, (2004), 825-830.

BEHAVIOUR OF STAINLESS STEELS IN SULPHATE-REDUCING BACTERIA (SRB) ENVIRONMENTS

V. Matres, E. Quirós

ACERINOX, S. A.

Abstract

The microbiologically induced corrosion (MIC) on the metal surfaces has been regarded as a serious problem in the last years, and the sulphate reducing-bacteria (SRB) influence is among the most famous cases. The SRB metabolism produces substances that can modify the environment (pH, oxygen and sulphide concentrations, conductivity, etc.), changing the reaction with the metal in contact.

In order to reveal the effect of this bacterial environment on the stainless steel, electrochemical and immersion tests were performed to compare six types of stainless steel (EN 1.4301, 1.4301 (mod.), 1.4401, 1.4565, 1.4539 and 1.4462) in different solutions, with or without SRB. The influence of the sulphides was reaffirmed by means of the electrochemical tests using SRB cultures, and the global environment effect of these bacteria was evaluated with immersion tests, where a visible bio-film is formed in a specific number of samples, causing surface changes. Clear differences among the surfaces are observed in the immersion tests, where the importance of the bacterial environment on the metal surfaces is visible.

Introduction

In the case of stainless steels and other ferrous alloys, the sulphate reducing-bacteria (SRB) are one of the most famous cases in the microbiologically induced corrosion (MIC), because they live in a great variety of industrial environments. Some theories explain the SRB mechanism but the W. Kuhr & Co [1, 2] theory is the best received. In this theory, the bacteria generate a cathodic depolarization, producing hydrogen and activating a reduction of inorganic sulphates to sulphides.

An example of the sulphide effect in the stainless steel observed is shown in the curves in Figure 1, recorded for the EN 1.4301 austenitic stainless steel in an aqueous environment, where different sodium sulphide concentrations were added.

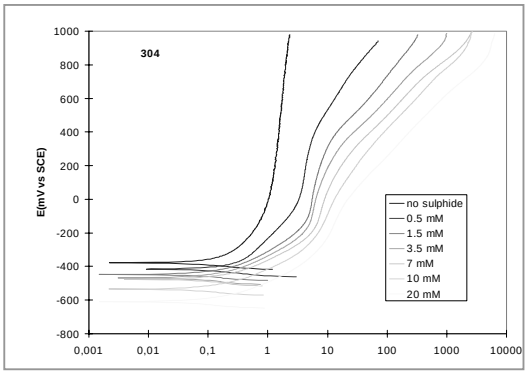

Figure 1. E vs. I curves for an EN 1.4301 austenitic SS in an electrolytic solution with different sulphide concentrations.

It is observed that the passivation intensity (i_p) increases and the corrosion potential decreases with the rise in sulphide concentration. Then, if the sulphide concentration grows in the environment, it will have a worst effect for the material in contact.

However, the sulphide presence is not the only negative factor for the stainless steel surfaces. In general, the bacteria colonies generate metabolic products, changing the environmental conditions on the metallic surfaces (pH, oxygen concentration, conductivity, etc). These changes can accelerate the corrosion process in the material and the possibility of a passive attack produced by the biomass exists because covered zones are generated where concentrations of batteries, ionic or heat transfers, etc. may be present.
A laboratory immersion test was carried out to know the global effect of the SRB environment, using a habitat of these bacteria in contact with some types of stainless steels. This SRB habitat will have all the metabolic substances that the bacteria produce in the course of the experiment, including sulphides.

Test material

The codes and the chemical compositions of the stainless steels investigated are given in Table 1.

Table 1. Identification and chemical composition of the studied materials.

DESIGNATION		**% WEIGHT**								
According to the test (**n**)	According to Euronorm	**Si**	**Mn**	**Ni**	**Cu**	**Cr**	**Mo**	**C**	**S**	**N**
1	EN-1.4301	0.37	1.75	8.04	0.2	18.23	0.17	0.044	0.001	0.055
2	EN-1.4301(mod)	0.30	0.78	7.96	0.42	18.18	0.36	0.042	0.001	0.123
3	EN-1.4401	0.41	1.18	10.67	0.31	16.90	2.19	0.039	0.002	0.043
4	EN-1.4565	0.25	5.63	17.85	0.14	24.47	4.60	0.025	0.001	0.450
5	EN-1.4539	0.16	1.66	24.32	1.53	20.43	4.57	0.020	0.001	0.078
6	EN-1.4462	0.34	1.74	5.70	0.16	22.65	3.13	0.022	0.001	0.156

Tests carried out in the study

In this study, the Hungarian Academy of Sciences supplied the SRB [Desulfovibrio desulfuricans (ATCC 7757)]. The SRB has been cultured by IRNAS-CSIC (Seville; Spain) in a culture solution prepared without oxygen, containing approximately 10^7 cells/ml.

A litre of the culture solution has the ingredients as follows:
Distilled water (1 L); K_2HPO_4 (0.5 g); NH_4Cl (1.0 g); Na_2SO_4 (1.0 g); $CaCl_2 \cdot 2\ H_2O$ (0.1 g); $MgSO_4 \cdot 7\ H_2O$ (2.0 g); DL–Na–Lactate (2.0 g); extract of yeast (1.0 g); Resazurin (1.0 g); $FeSO_4 \cdot 7\ H_2O$ (0.5g); ascorbic acid (0.1 g); Na-Thioglycolate (0.1 g).

Electrochemical tests

Before the immersion test, the SRB effect was studied in electrochemical tests, using a hand-made corrosion cell (Avesta type design). In this cell, 300 ml of the culture solution is homogenised with mechanical stirring, and a flow of N_2 (0.8 l/min) eliminate the presence of oxygen.
The reference electrode is a saturated calomel electrode (SCE), and the counter electrodes are two graphite bars and the work electrode is a stainless steel specimen.
Using an upward polarisation technique, the electrochemical curves of each material are studied in the anodic zone. The potential scanning begins in 50 mV vs. OC (*Open Circuit*) and the scan rate is 1 mV/s.
All the studied materials present an increase in the passivation intensity with the increase of sulphide in the environment. An example is shown in Figure 2 with some of the obtained electrochemical curves for the EN 1.4301 stainless steel.

The sulphide concentration produced by the SRB is checked in each culture before the tests and it is indicated for each one.

In order to observe the influence of high sulphide concentrations, sodium sulphide is added in some cultures.
In Figure 3, the curve obtained for the EN 1.4301 material in a culture with 483 ppm of sulphide is compared with the same material in a blank culture (culture solution without SRB). In Figure 4, the behaviour of all the stainless steels studied in cultures with sulphide added (480-530 ppm S^{2-}) is illustrated. A large increase in the current intensity is detected for all the stainless steels. The corrosion potential is very similar in all steels, but the passivation intensities are somewhat different. According to these results, the EN 1.4301 is the less resistant and the EN 1.4462 is the stainless steel with greater resistance in these conditions. The results obtained up to now indicate that the sulphide is detrimental for the stainless steel.

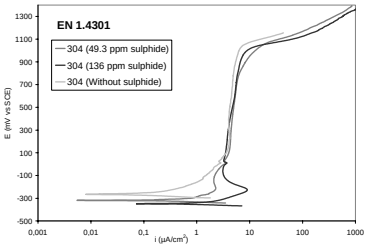

Figure 2. EN 1.4301 electrochemical curves in SRB cultures with **0**, **49.3** and **136** ppm S^{2-}.

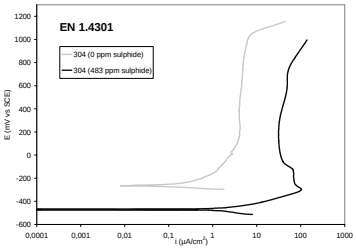

Figure 3. EN 1.4301 electrochemical curves in SRB cultures with Na_2S added.

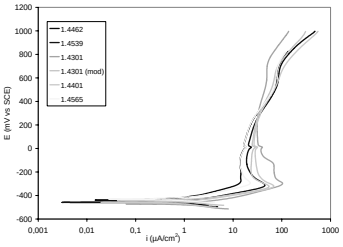

Figure 4. Electrochemical curves of all the materials in SRB cultures with Na_2S added.

Immersion test

In the immersion test, the samples are submerged in different solutions with or without SRB during a long period of time. This test tries to simulate what would happen in a field test.

Selected test environments

Six different solutions were used (Table 2), where three variables were considered: 1) the base solution; 2) the sulphide concentration; and 3) the presence or not of sulphate-reducing bacteria (SRB).

Table 2. Environments used in the immersion testing

Identification (X)	Environments for the immersion of the samples
A	CULTURE SOLUTION WITHOUT BACTERIA (No SRB); [Blank]
B	CULTURE SOLUTION + **SRB**
C	CULTURE SOLUTION + **SRB** + 150 ppm NaS
D	CULTURE SOLUTION + **SRB** + 300 ppm NaS
E	FRESH WATER + 150 ppm NaS
F	FRESH WATER + 300 ppm NaS

A litre of fresh water (simulation of the river water) contains the following compounds (concentrations x 10^{-3}):
NaCl (5.02 g/l); $MgSO_4 \cdot 7H_2O$ (0.14 g/l); $NaNO_3$ (0.02 g/l); K_2SO_4 (0.02 g/l); K_2HPO_4 (0.001 mg/l); NH_4Cl (0.0003 mg/l); $NaNO_2$ (0.0001 mg/l); $FeCl_2 \cdot 4H_2O$ (0.001 mg/l); $MnCl \cdot 4H_2O$ (0.0001mg/l); HCl (0.4 mM); $CaCl_2 \cdot 2H_2O$ (0.0004 g/l); $NaHCO_3$ (0.0008 g/l).

Test procedure

Four samples (75 x 35 mm^2) from each material were cut with a cut shear and the edges were ground to eliminate any burs. The samples were partially submerged in dull plastic glasses with 80 ml of the test solution (Figure 5), except the samples in the blank solution (only 20 ml). After introducing the samples, the glasses were closed hermetically.

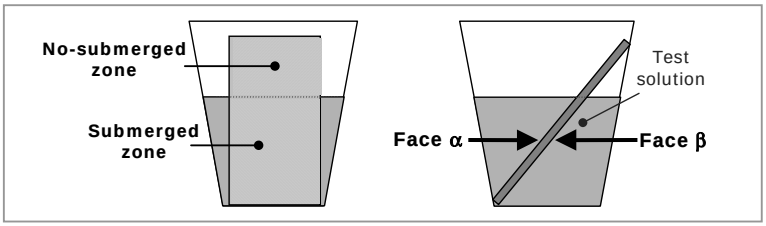

Figure 5. Diagram with the samples inside the glasses.

Two evaluations were carried out with each material. The first one was done after five months from the beginning of the test and the second one nine months later. Two different zones existed in the samples: the submerged zone and the non-submerged zone.

Test evaluation

The appearance observed by the different samples after a simple rinse is presented in Figures 6, 7, 8 and 9. The samples were identified as nXx: **n**= 1-6 (Material type; table 1); **X**= A-F (Test solution; table 2); **x** = a-d (Repetition of the same material and test solution).

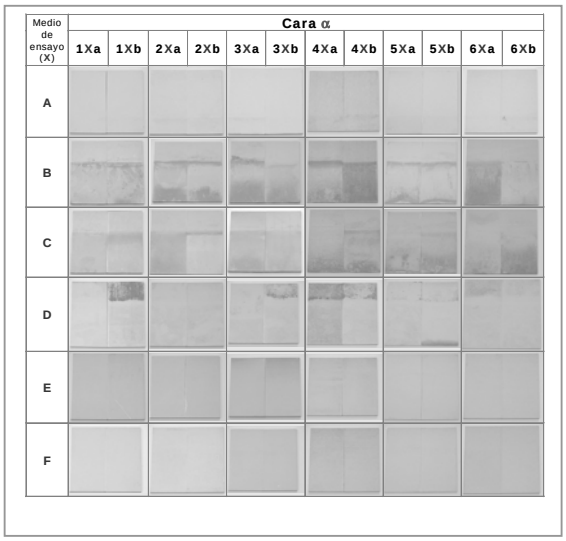

Figure 6. Appearance of the samples (α face) after **5 months**

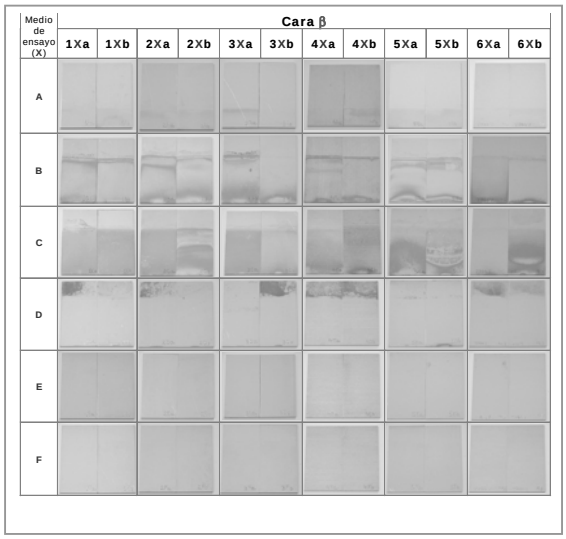

Figure 7. Appearance of the samples (β face) after **5 months**

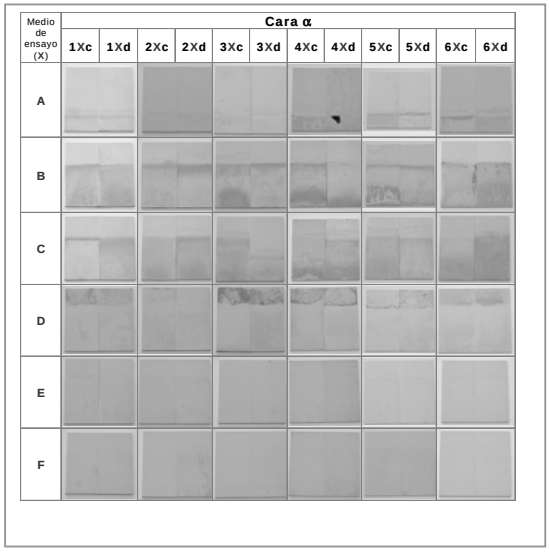

Figure 8. Appearance of the samples (α face) after **9 months**

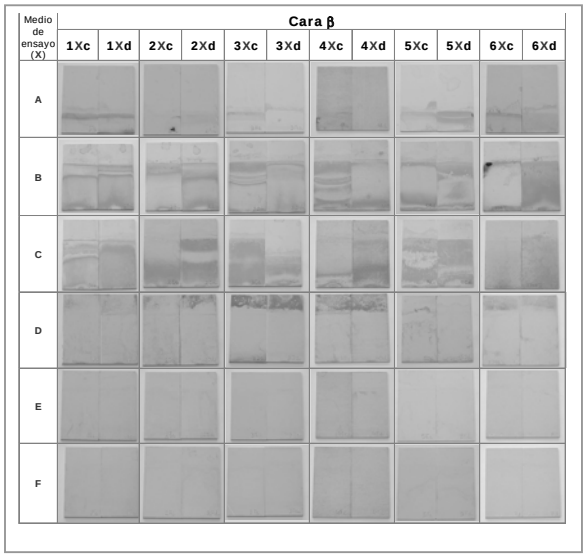

Figure 9. Appearance of the samples (β face) after **9 months**

The overall evaluation of the samples, based in the visual appearance, is similar for both periods of exposition time. It seems the less affected samples are the samples submerged in fresh water (solutions **E** and **F**), where the mark of the gas-liquid interface zone is almost imperceptible on the surface. The samples exposed to the culture solution without bacteria (solution **A**) have presented a surface change lightly more perceptible. In all cases, the submerged zone is darker than the non-submerged. The culture solutions with bacteria (solutions **B**, **C** and **D**) are the environments with greater effect on the sample surfaces.

A similar effect is observed in the samples with the solutions **B** and **C**, where the non-submerged zone is not affected at first sight. Some deposits in the interface area and a colour visual effect in the submerged zone are seen. The colour effect is also found in the surface zone in contact with the bottom of the glass. Most of the deposits observed in the interface area and submerged zone are easily eliminated with water and lightly rubbing with latex gloves, using acetone in a deeper cleaning. But the colour effect cannot be eliminated with the non-aggressive cleaning methods used (hot hydrogen peroxide; alcohol (ethanol); acetone).

Curiously, the effect of the solution **D** is opposite to the **B** and **C** environments. In this case, the non-submerged zone is the most affected, with a film of greyish residues. However, the submerged zone has not much surface changes (only some darkening in some parts).

The final cleaning of all the samples let observe that no pits in the surfaces appear. The total sulphide concentration of each solution after the evaluations using Induced Coupled Plasma spectroscopy (ICP) and pH have been determined at the end of the test (after 9 months).

Table 3. Sulphide concentration and final pH.

MATERIAL	Sulphide concentration (ppm)			Final pH
	Initial	After 5 months	After 9 months	
A	0	0	0	8.51
B	51-59	9-11	2-6	8.58
C	71-164	7-11	3-8.3	8.43
D	321-352	3-5	0.5-1	8.83
E	160	0	0	9.44
F	311	0	0	10.46

The final concentration of sulphide for each evaluation is very different to the initial value (except in solution A). It is important to see that the environments with SRB are the only ones with sulphide at the moment of the evaluation. The difference in sulphide could have some causes. One reason would be that the sulphide in aqueous solution turns into hydrogen sulphide (H_2S). This volatile compound would stay in the top of the glass and would leak in the moment of the opening (sample evaluations). A second reason could be favoured by the pH of the solutions: The sulphide turns into sulphates, thiosulphates, sulphites, etc., because of the aerobic conditions of the test (although without oxygen renovation, favoured for the immobility of the solutions and the hermetic seal of the glasses). According to the literature, this is not an obstacle for the survival of the bacteria, because the SRB could survive even with high aerobic conditions. This fact could explain why the environments with sulphide at the end of the test would be the environments with SRB. This is a sign of the bacterial activity in the culture solutions. If the residual sulphide detected would be due to the SRB activity, the fact that environment with more sulphide added (D) have less residual sulphur respect to environments B and C could indicate that great sulphide concentrations would be harmful for the bacteria.

Conclusions

The bacterial influence is detected in the surface changes (residues, colour effect) on the samples. These changes are generated by the presence of a biofilm on the stainless steel surface.
This effect of the biofilm on stainless steel surface and the gas-liquid interface is affected by sulphide concentration.

References

[1] G. Kobrin, “Corrosion by microbiological organisms in natural waters”, Materials performance. July 1976. 38-43, p. 365-370. National association of corrosion engineers.

[2] G. Geesey, “What is biocorrosion?”, Biofouling and biocorrosion in industrial water systems. Proceedings of the international workshop on industrial biofouling and biocorrosion. Stuttgart. Sept. 13-14, 1990

[3] R.E. Tatnall, “Case histories: Biocorrosion”, Biofouling and biocorrosion in industrial water systems. Proceedings of the international workshop on industrial biofouling and biocorrosion. Stuttgart. Sept. 13-14, 1990

[4] H.A. Videla, “Interpretación bioelectroquímica de la ruptura de la pasividad del acero al carbono por bacterias sulfatorreductoras”, Revista Iberoamericana de corrosión y protección, Vol. XXII, No.1, 1991

[5] M. Eashwar. P. Chandrasekaran. G. Subramanian. K. Balakrishnan, “Microbiologically influenced corrosion of steel during putrefaction of seawater: Evidence for a new mechanism”, Corrosion. Vol. 49, No. 2, 1993, p. 108-113

[6] P. Angell. J.S. Luo. D.C. White, “Microbially sustained pitting corrosion of 304 stainless steel in anaerobic seawater”, Corrosion Science, Vol. 37, No. 7, 1995, p. 1085-1096.

HYDROGEN CORROSION OF STAINLESS STEELS

K. Lublinska, A. Szummer, K. Szpila, K.J. Kurzydłowski

Warsaw University of Technology, Poland

Abstract

In this work detailed investigations on the microstructural changes, which take place as a result of cathodic hydrogen charging in sulphuric acid solution, in the ferritic, austenitic and duplex steels, have been carried out. The applied experimental techniques included LM (light microscopy), SEM (scanning electron microscopy) and TEM (transmission electron microscopy). Electrochemical measurements were performed to determine the influence of hydrogen ingress on the corrosion resistance. It was found that cathodic hydrogen charging causes significant changes in the microstructure of the materials studied. In these three stainless steels hydrogen ingress has caused a substantial increase of dislocation density. This in turn leads to a decrease in the localized corrosion resistance, particularly pitting. Hydrogen ingress to stainless steels also causes deterioration of their plastic properties. The mechanisms of the observed phenomena are also discussed.

Introduction

Hydrogen has a disadvantageous effect on a number of structural steels. This negative effect of hydrogen on metals is described as hydrogen corrosion or hydrogen embrittlement. Stainless steels undergo an embrittlement by hydrogen in aqueous media and in hydrogen atmosphere, but the mechanism of the ductility loss has not been explained satisfactorily until now [2, 4, 9]. Due to the industrial accidents, the hydrogen embrittlement remains as a serious problem for scientists and engineers alike. Ferritic stainless steels in general are more affected by hydrogen than austenitic ones. It is partly due to generally a lower yield strength, their higher hydrogen solubility and lower tendency to hydrogen segregation of austenitic steels [4, 9].
It is well known that hydrogen induces degradation of the microstructure and mechanical properties of stainless steels [1-11]. The mechanisms of hydrogen degradation are complex and numerous investigations have not, as of yet clarified them sufficiently. The role of hydrogen in the process of corrosive failure in steels is also far from being fully understood currently, a general consensus has been reached that. In investigation of degradation of the properties, it is necessary to take greater account of the structural changes brought about by hydrogen.

The aim of this work was a detailed description of the changes, which take place as a result of hydrogen ingress, in the microstructure of stainless steels and of the mechanism and influence of such changes on resistance to corrosion and on their plastic properties.

Materials and Experimental Procedure

Commercial austenitic, special low carbon ferritic and duplex (semi austenitic) stainless steels having the compositions shown in Table 1 were used for the present study. Single crystals of steel containing 16 wt.%Cr were also studied.

Hydrogen cathodic charging was carried out at 0.05A/cm^2 or 0.1 A/cm^2 for 3 to 18 hours at ambient temperature, with platinum anode in 0.5M H_2SO_4 solution containing 1 mg As_2O_3 per dm^3 as a hydrogen recombination poison. For microstructure examinations, samples before and after hydrogen charging were examined using light (LM), scanning (SEM) and transmission electron (TEM) microscopy.

Table 1. Chemical composition (weight %) of the steels investigated

	C	S	Cr	Ni	Mn	Si	Mo	Ti
Type 304	0.051	0.021	18.37	10.18	1.5	0.43	0.03	
Type 310S	0.11	0.005	25.83	19.61	1.13	2.52	0.16	
Type 304L	0.019	0.022	19.04	11.76	1.50	0.56	0.08	
Type 316L	0.031	0.005	17.07	11.95	1.55	0.48	2.65	0.37
Duplex 19Cr 5Ni	0.042	0.019	17.9	4.90	0.28	1.72	2.65	
Type 410S	0.019	0.001	12.27	0.16	0.27	0.34	0.02	
Type 430L	0.025	0.011	19.3	0.15	0.36	0.41		0.41
Single crystal 16Cr	0.06	0.014	16.0			0.1		

The effect of hydrogen on the mechanical properties of stainless steels has been investigated by the slow strain rate technique (SSRT). Specimens were tensile tested to failure while undergoing cathodic charging or in air. Uniform elongation (A) was used to determine the ductility of the samples.

In order to reveal the influence of hydrogen on corrosion resistance to pitting corrosion, electrochemical tests have been carried out by the potentiodynamic method in 0.5M NaCl solution, in room temperature.
The scanning electron microscopy (SEM) was employed to describe changes in the fracture surface or the pitting morphology caused by hydrogen.

Results and Discussion

Metallographic examinations of samples before and after cathodic charging revealed that cathodic hydrogen causes significant and permanent changes in the microstructure of all steels investigated in this work, particularly in the surface layer of the specimens.

In all austenitic stainless steels, after hydrogen charging, the initially smooth electropolished surfaces reveal numerous microcracks and blisters with microcracks – Figure 1. Both transgranular (parallel) and grain boundary microcracks were observed as shown in Figure 1a. Those surface cracks develop in austenitic stainless steels subjected to cathodic charging in the absence of externally applied stresses. The hydrogen-induced microcracks observed on the surface of the electrolytically H-charged specimens form mainly during post-process aging, i.e. during hydrogen egress [1, 2, 8, 10]. They initiate as a result of the formation of hydride phases, which are unstable under normal atmospheric conditions [1, 2, 8, 10, 11].

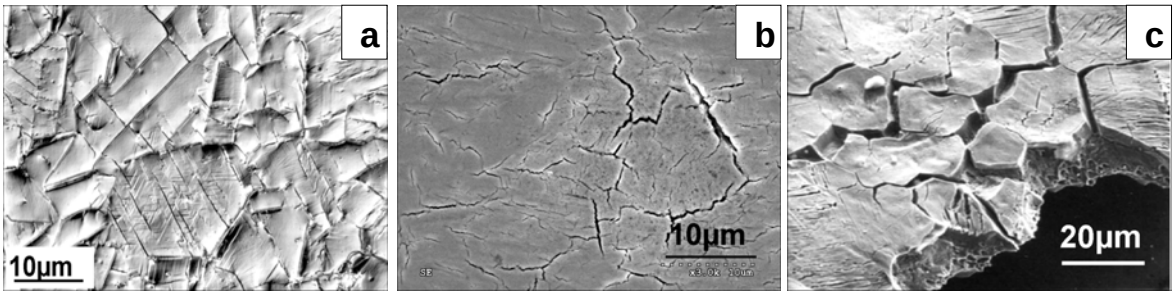

Figure 1. (a) –Surface of the solution annealed Type 316L austenitic stainless steel (LM, Nomarski contrast) for an unetched H-charged sample. (b) H-induced microcracks on the surface of Type 304L steel, SEM. (c) SEM image of 310S steel after cathodic hydrogen charging, a tensile test sample – decohesion at grain boundaries in the brittle hydrides layer.

These hydrides constitute a hard and brittle surface layer, several micrometers thick with numerous microcracks (Figure 1c). They decompose when charging is stopped. During storage at room temperature in air, the hydrogen escapes, and within several hours the hydrides entirely disappear [1, 2, 8]. Decomposition of hydrides occurring during aging at room temperature produces high local multiaxial tensile stresses [1, 2, 8, 10].

The harmful influence of cathodic hydrogen was also observed in ferritic steels [3, 5, 6, 7]. The changes in the microstructure are particularly intensive in the surface layer, the thickness of about 10μm. In this layer, needle-like microtwins form with the characteristic surface relief similar to the acicular martensite, in the absence of $\gamma - \alpha$ transformation (Figure 2). TEM examinations of specimens after hydrogen charging revealed regions with high dislocation density and hydrogen-induced microtwins (Figure 3) [3].

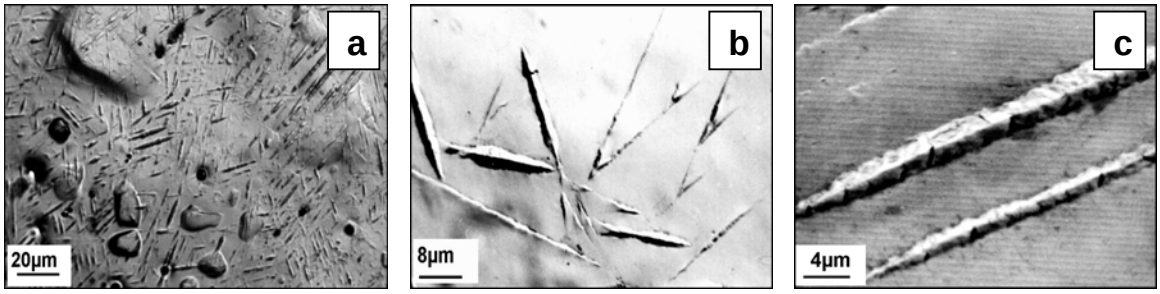

Figure 2. H-induced grain oriented microtwins in the form of needles and blisters on the surface of 430L ferritic steel (a) and in the single crystal of 16Cr ferritic steel – (b, c)

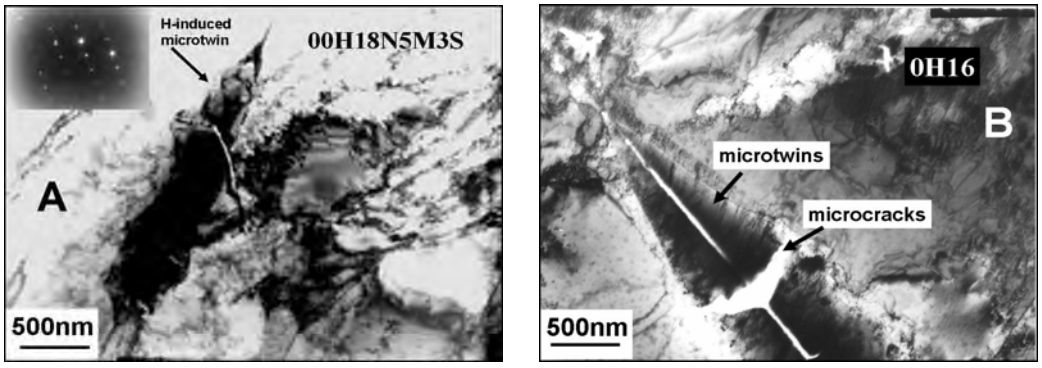

Figure 3. High internal dislocation density surrounding microtwins revealed in TEM images of microtwins with microcracks in a ferrite grain of duplex steel (A) and in the single crystal of 16Cr ferritic steel (B)

In addition, hydrogen-induced microcracks, crevices and blisters with microcracks were found – Figure 4a, b, c, d. Microcracks cross the needles and some of them run along the midribs (Figure 3). Hydrogen corrosive damage was also found at deeper layers, especially along grain boundaries and at non-metallic inclusions (Figure 4e, f). The observed hydrogen induced microcracks in ferrite grains and in microtwins might be caused not only by hydrogen trapping, but also generally high stresses caused by an increase of the lattice constant due to hydrogen dissolution in ferrite [7].

In the duplex stainless steel, the corrosive changes brought about by hydrogen are of mixed character: in ferrite – similar to those observed in ferritic steels, and in austenite – typical of those in austenitic steels. The microtwins only form in ferrite grains (Figure 5a).

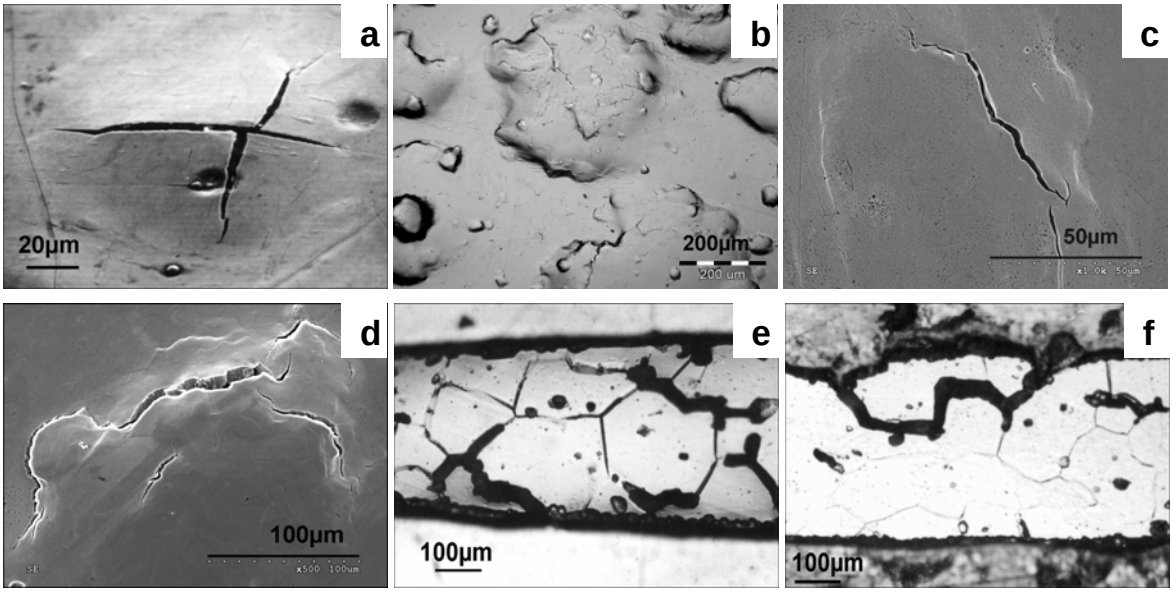

Figure 4. Hydrogen-induced blisters with microcracks on the surface of the single crystal of 16Cr ferritic steel (a) and in 410S ferritic steel (b, c, d). Microcracks and crevices at deeper layers in the 19Cr ferritic steel after hydrogen charging, specimens etched electrolytically – (e, f)

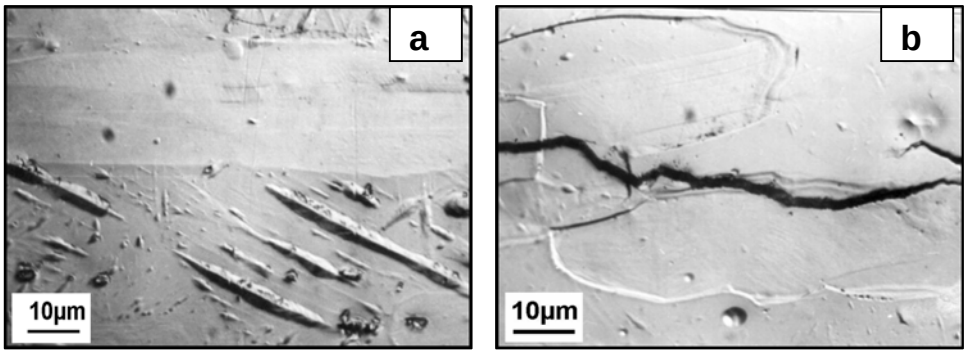

Figure 5. Hydrogen induced microtwins in ferrite-phase grain (a) and cracks (b) in 19Cr5Ni duplex steel

Hydrogen charging lowers the resistance to a local corrosion of ferritic and austenitic stainless steels. It reduces the protective properties of the passive layers, and the surface defects become preferred places for initiation of corrosion pits in the solutions containing chlorides.

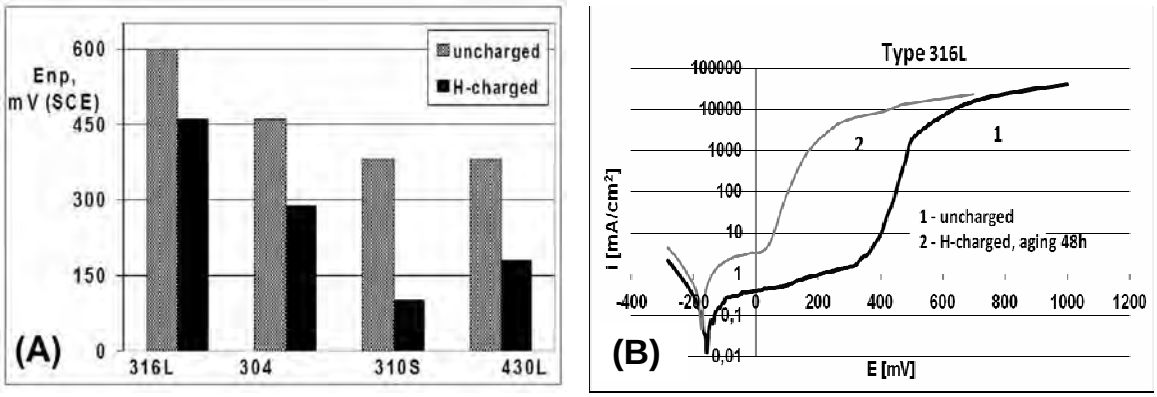

Figure 6. Enp values for the stainless steels before and after H-charging in borate buffer + 0,1M NaCl solution (A). Some examples of anodic polarization curves for hydrogen charged and uncharged samples of 316L stainless steel in 0.5M NaCl solution (B)

Figure 6a shows Enp (potential of passivity breakdown) for samples before and after H-charging. The uncharged steels exhibit Enp distinctly higher than that for H-charged samples. In corrosion tests it was found that initially, prior to charging, pits nucleate in stainless steels exclusively at non-metallic inclusion (Figure 7a). On the other hand, in hydrogen charged samples the hydrogen–induced microcracks and blisters are particularly sensitive sites for pitting corrosion (Figure 7 b, c, d, e, f). Especially in the austenitic stainless steels the pits nucleate easier on microcracks –
Figure 7d, e, f.

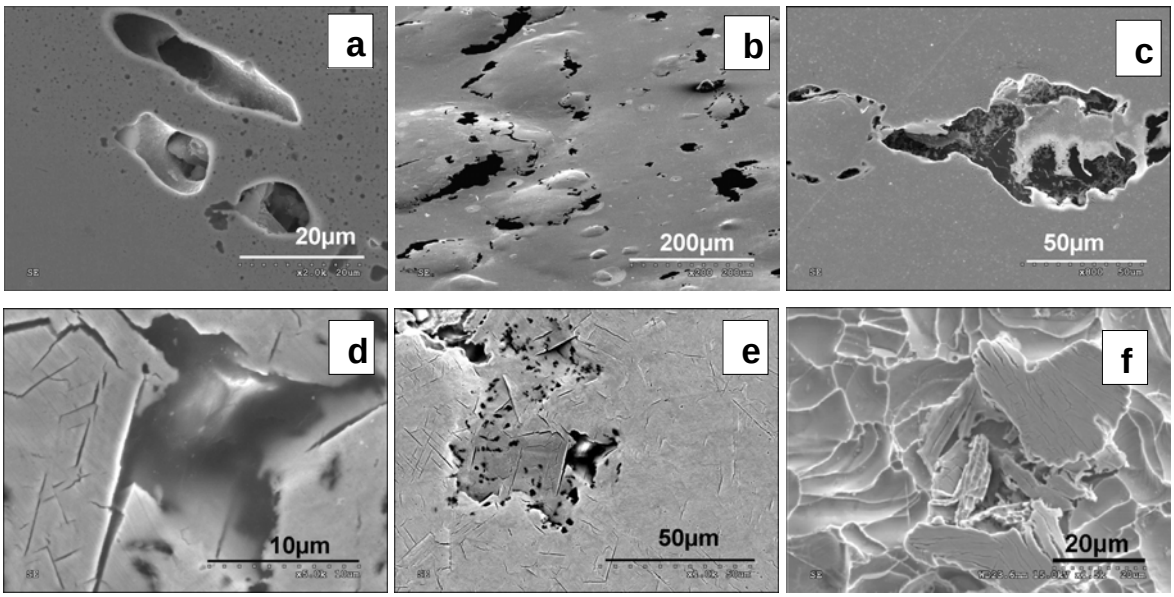

Figure 7. Surface of stainless steels after corrosion testing (0.5M NaCl) of uncharged (a) and of hydrogen charged specimens (b÷f). (a) – pit nucleation at non-metalic inclusions in unchanged 304L. (b, c) – localized corrosion attack at the hydrogen-induced blisters on the surface of 410S. (d, e) – initial stage of pits formation at hydrogen-induced microcracks in the 316L and in the 304L (f) steels

Hydrogen ingress to stainless steels also leads to detorioration the mechanical properties and their plastic properties.

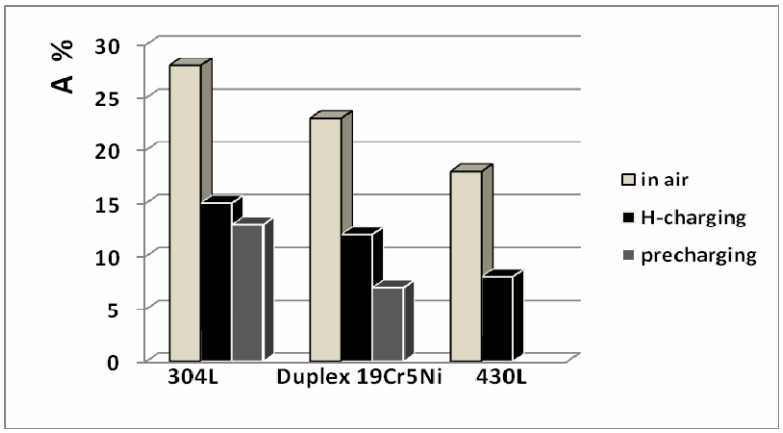

Figure 8. Reduction of the elongation to fracture (A) in H-charged stainless steels tensile tested in various conditions: 1 – in air, 2 – charging during tensile test, 3 – precharging before tensile test in air

Hydrogen charging substantially reduces the ductility of the investigated steels, (see Figure 8) and leads to brittle fractured surface with secondary cracks – (Figure 9 b). In the non-charged samples the fracture surface remains ductile – (Figure 9 a). SEM observations of the tensile tested samples revealed the presence of wide cracks on the lateral surfaces, close to the fracture – (Figure 9 c). These large cracks start at the first H-induced microcracks (Figures 9d, e, f).

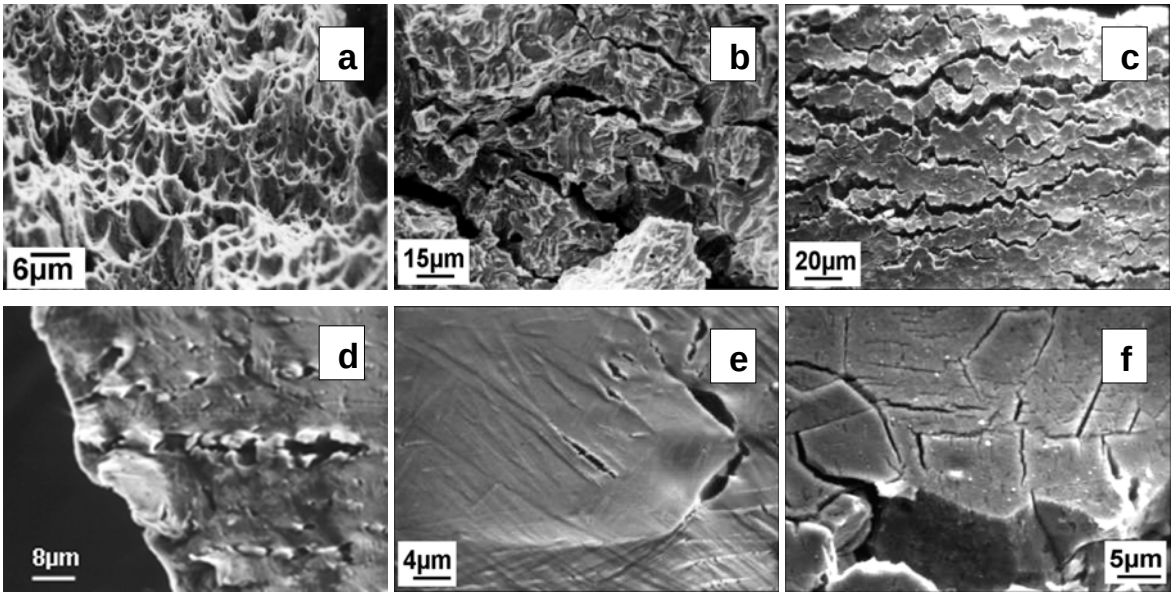

Figure 9. Ductile fracture surface in sample of 304L steel tensile tested in air (a). Tensile tested samples during H-charging (b÷f). Brittle fracture surface of 304L steel (b). Large cracks on lateral surface of 304L steel (c). The initial stage of growth cracks at the H-induced microcracks in 430L (e) and in 304L (f)

Conclusions

Hydrogen degrades the microstructure of the ferritic, austenitic and duplex stainless steels. Surface microcracks and blisters can be observed by SEM. TEM investigations reveal microtwins and an increased density of dislocations. All these changes in extreme cases can lead to a significant deterioration of the material properties, especially the mechanical properties and of the corrosion resistance.

Acknowledgments

This work was supported by Polish Ministry of Science and Higher Education as the research project PBZ KBN-117/T08/2005.

References

[1] K. Kamachi. Transactions ISIJ, 18, (1978), 485-491.
[2] SN. Narita, C.J. Altstetter, and H.K. Birnbaum, Metall. Trans. A, 13A, (1982) 1355.
[3] A. Szummer, K. Lublińska, E. Jezierska, Microstructural Science, 23, (1996), 141-147.
[4] P. Timmins, Solutions to Hydrogen Attack in Steels, ASM, Mat. Park, USA, (1997).
[5] M. Taninio, H. Komatu, S. Funaki, Journal de Physique, 43, (1982), c4-503.
[6] A. Szummer, E. Jezierska, K. Lublińska, J. Alloys and Compounds, 293-295, (1999), 356.
[7] K. Lublińska, A. Szummer, K.J. Kurzydłowski, Surface Engineering, I2A, (2005),167.
[8] A. Szummer, in Hydrogen Degradation of Ferrous Alloys, Noyes Publications, Park Ridge, New Jersey, U.S.A., (1985), 512.
[9] T.J. Carter, L.A. Cornish, Engineering Failure Analysis, 8, (2001), 113-121.
[10] M. Holzworth and M. Louthan, Corrosion, 24, (1968), 110.
[11] S.A. Inoue, V. Hosoya and T. Masumoto, Trans. Iron Steel Inst. Japan, 19, (1979), 170.